

Lattice dynamics of mixed semiconductors (Be,Zn)Se from first-principles calculations

A. V. Postnikov*

*Institute of Metal Physics, S. Kowalewskoj 18, Yekaterinburg 620219, Russia,
and Universität Osnabrück – Fachbereich Physik, D-49069 Osnabrück, Germany*

Olivier Pagès, Joseph Hugel

Université de Metz - Institut de Physique, 1 Bd Arago, F-57078 Metz cedex 3, France

(Dated: March 24, 2021)

Vibration properties of $\text{Zn}_{1-x}\text{Be}_x\text{Se}$, a mixed II-VI semiconductor characterized by a high contrast in elastic properties of its pure constituents, ZnSe and BeSe, are simulated by first-principles calculations of electronic structure, lattice relaxation and frozen phonons. The calculations within the local density approximation has been done with the SIESTA method, using norm-conserving pseudopotentials and localized basis functions; the benchmark calculations for pure endsystems were moreover done also by all-electron WIEN2k code. An immediate motivation for the study was to analyze, at the microscopic level, the appearance of anomalous phonon modes early detected in Raman spectra in the intermediate region (20 to 80%) of ZnBe concentration. This was early discussed on the basis of a percolation phenomenon, i.e., the result of the formation of wall-to-wall –Be–Se– chains throughout the crystal. The presence of such chains was explicitly allowed in our simulation and indeed brought about a softening and splitting off of particular modes, in accordance with experimental observation, due to a relative elongation of Be–Se bonds along the chain as compared to those involving isolated Be atoms. The variation of force constants with interatomic distances shows common trends in relative independence on the short-range order.

PACS numbers: 63.20.-e, 63.50.+x, 71.15.-m, 71.55.Gs, 78.30.-j

I. INTRODUCTION

(Be,Zn)Se is an example of mixed II-VI semiconductor system whose electronic properties and, consequently, elastic characteristics vary with concentration in a non-trivial way. A considerable effort has been spent on characterizing the optical band gap, which drops slightly from intermediate concentrations and undergoes a change from direct to indirect character underway from ZnSe to BeSe¹. Not less interesting possibilities open in the tuning of elastic properties, because BeSe and ZnSe, similarly to some other easily miscible II-VI constituents, possess quite different elastic constants, which have to be accommodated in a solid solution. (Be,Zn)Se makes, actually, quite an extreme case of elastic contrast between constituents in a mixed system. This was argued to favor the appearance of anomalous lines in the Raman spectra, which split off on the soft side of the BeSe-related TO peak in the $x \sim 0.2\text{--}0.7$ concentration range of $\text{Be}_x\text{Zn}_{1-x}\text{Se}$ crystals, as was detected by Pagès *et al.*². In order to explain this anomaly, Pagès *et al.*³ brought into discussion an idea of quasi-infinite chains, which are developing in the softer matrix (ZnSe) as the BeSe concentration reaches the percolation threshold of $\sim 20\%$. However, the microscopic mechanism relating percolation with vibration properties remained speculative. The present work's aim is to provide a possible complete and reliable first-principles description of internal tensions, structural relaxation, and the impact of the latter on lattice-dynamical properties of a mixed $\text{Be}_x\text{Zn}_{1-x}\text{Se}$ alloy near the percolation threshold. A concise result of our simulation has been reported earlier as a conference

proceeding⁴. Here we offer a detailed outline of results obtained for different supercells, with a more lengthy discussion. In particular, we provide an analysis of bond lengths distribution for a number of compositions, discuss the change of force constants related with that, and finally calculate phonon density of states and provide its the wavevector-resolved decomposition.

The electronic properties of pure constituent compounds are well known; they also were probed by *ab initio* methods of respectful accuracy in a number of earlier publications. Simulations of comparable accuracy on mixed alloys are seriously complicated by the necessity to treat large supercell, with a practical loss of any useful symmetry. A certain success has been achieved in molecular dynamics (MD) simulations of an isostructural III-V mixed semiconductor alloy, (Ga,In)As: Branicio *et al.*⁵ performed parametrized MD calculations for supercells with up to 8000 atoms, and *ab initio* MD calculations on 216-atom supercells. We are not aware of any elastic simulations on mixed II-VI semiconductors but that by Tsai *et al.*⁶, who used multicenter MD method, a formally *ab initio* one but of inferior accuracy to the method applied here. Comparing our results with those of Tsai *et al.*, we find an overall good agreement, albeit with quantitative discrepancies on some sensitive issues. A more important difference is, however, that we study more attentively the limit of low Be concentration, particularly the onset of percolation on the Be sublattice. Moreover, we calculate phonon densities of states and discuss them in immediate reference to experimentally obtained Raman spectra.

The paper is organized as follows. In Sec. II we outline our *ab initio* calculation approach to electronic structure and vibration properties. Sec. III, containing the results

for pure endsystems ZnSe and BeSe, is concise in view of numerous previous studies, but it is necessary here in order to assess the accuracy of the calculation method. In Sec. IV we outline our results for lattice parameters and equilibrium bond lengths in relaxed supercells, simulating a broad concentration range. The effect of bond lengths on the force constants between nearest and next-nearest neighbors is discussed in Sec. V. Finally, the manifestation of the force constants in phonon frequencies is explained in Sec. VI, along with the discussion on wavevector dependency and vibration patterns in different parts of the phonon spectrum.

II. CALCULATION SCHEME AND SETUP

Dynamical properties are derived from the total energy or forces, which are evaluated *ab initio* in a sequence of density functional calculations. We applied the calculation method, and computer code, SIESTA⁷, which incorporates norm-conserving pseudopotentials in combination with atom-centered strictly confined numerical basis functions^{8,9}. The pseudopotentials were constructed along the Troullier–Martins scheme¹⁰ for the following valence-states configurations: Be $2s^2(2.0)$, Se $3d^{10}(1.2) 4s^2(1.9) 4p^4(2.0)$, Zn $3d^{10}(1.09) 4s^2(2.28)$. The numbers in brackets stand for pseudoization radii of corresponding states in Bohr. The basis set consisted of double- ζ functions with polarization orbitals in all l channels on all centers (Be $2s2p$, Zn $3d4s4p$, Se $3d4s4p$), hence also for explicitly included semicore Se $3d$ states. The details on the basis classification and testing in SIESTA can be found in Refs. 8,9. Our basis generation followed the standard split schema of the SIESTA code, with the energy shift parameter, responsible for the localization of basis functions, equal to 20 mRy. This resulted in basis functions with maximal extension of 3.17 Å (Be), 3.12 Å (Zn) and 2.82 Å (Se), i.e. well beyond the nearest-neighbor distances but short of direct overlap to next-nearest neighbors. The full structure optimization (of cell parameters and internal coordinates) was performed in all supercells prior to lattice dynamics calculations. In order to get reliable forces on atoms it is essential to accurately perform spatial integration of the (general-form) residual charge density over the unit cell. To this end, we used the mesh cutoff parameter of 250 Ry, that generated a real-space mesh with the step of about 0.1 Å along each Cartesian direction throughout the supercell. Within each mini-cell of this real-space mesh, an averaging of integration results was done over four fcc-type sampling points for better numerical stability. This resulted in the forces summing up, over all atoms in the supercell, to zero within the accuracy of ± 0.1 eV/Å, separately along each Cartesian direction. The thus validated forces were used to calculate the dynamical matrix elements, by introducing small (0.016 Å) deviations of atoms one by one from their equilibrium positions. The details of phonon calculations are discussed in Sec. VI.

All our SIESTA calculations have been done in the local density approximation (LDA). For the pure ZnSe and BeSe systems, moreover, we used the full-potential augmented plane wave method (see, e.g., Ref. 11), as implemented in the WIEN2k code¹². We apply here this all-electron method of recognized accuracy for benchmark calculations of elastic properties. We provide the WIEN2k results obtained both within the LDA and in the generalized gradient approximation (GGA, Ref. 13).

III. ENDSYSTEMS, ZnSe AND BeSe

The electronic structure of zincblende-structure semiconductors ZnSe and BeSe was extensively studied by both experimental means and first-principle calculations. Band dispersions and partial densities of states have been calculated in the LDA by Lee *et al.*¹⁴ and Agrawal *et al.*¹⁵ (for ZnSe, among other Zn chalcogenides) and by Fleszar and Hanke¹⁶ (for BeSe, among other Be chalcogenides). In the latter publication, also the quasiparticle band structure has been calculated in the *GW* approximation, and subsequently discussed in the context of LDA vs. *GW* and exact exchange for a number of *sp*

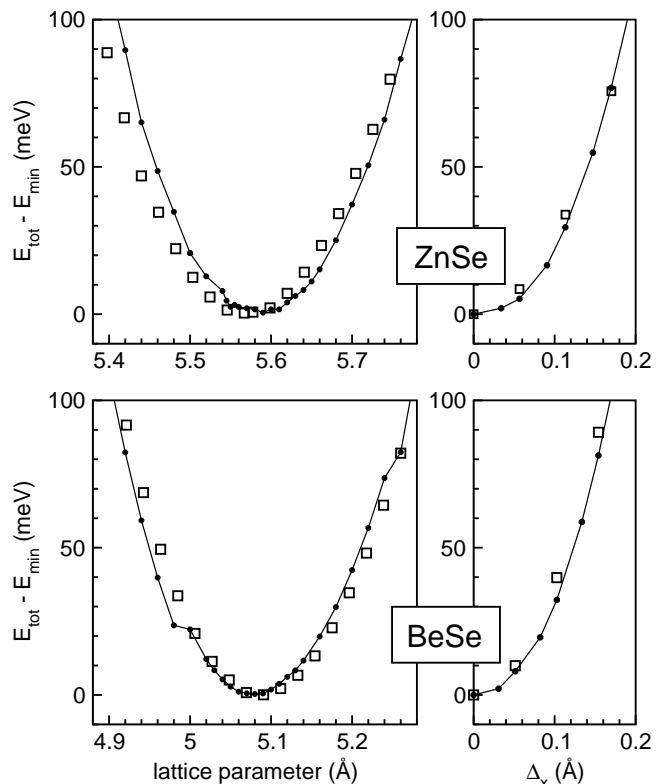


FIG. 1: The total energy vs. lattice constant curves (left) and the energy profiles corresponding to the Γ -TO phonon (right) as calculated for ZnSe and BeSe. Δ_x indicates the magnitude of the cation (or anion) displacement along [100] from the equilibrium. Open squares: WIEN2k (LDA) results; connected black dots: SIESTA (LDA) results.

TABLE I: Elastic properties of ZnSe and BeSe from experiments and first-principles calculations.

Method	ZnSe			BeSe		
	a (Å)	B (Kbar)	ω_{TO} (cm^{-1})	a (Å)	B (Kbar)	ω_{TO} (cm^{-1})
WIEN2k (LDA)	5.568	714	198	5.084	920	498
WIEN2k (GGA)	5.571	727	206	5.182	816	523
SIESTA (LDA)	5.587	758	203	5.078	912	500
exp.	5.668 ^a	624 ^b	207, ^c 205 ^d	5.137 ^e	920 ^e	501 ^d
other calc.	5.677, ^f 5.638, ^g 5.633, ^h 5.636 ^k	689, ^f 652, ^g 811, ^h 649 ^k	224 ^h	5.037 ⁱ	988 ⁱ	547 ^j

^aRef. 17^bRef. 18^cRef. 19^dRef. 20^eRef. 21^fLDA, norm-conserving pseudopotential with Zn3d as valence states, Ref. 22^gLDA, norm-conserving pseudopotential with Zn3d and Se 3d as valence states, Ref. 14^hLDA, full-potential LMTO, Ref. 15ⁱLDA, norm-conserving pseudopotential, Ref. 23^jLDA, norm-conserving pseudopotential, Ref. 24^kfull-potential LMTO, Ref. 25

zincblende semiconductors²⁶. For ZnSe, the quasiparticle band structure has been reported by Luo *et al.*²⁷. Our calculations provide the band structures in agreement with good earlier LDA results, so we skip the discussion on this point. Instead we turn to elastic properties and note that the optimized ground-state volume along with the bulk modulus have been reported in many calculations for ZnSe (see Table 1), and also by Muñoz *et al.*²³ and González-Díaz *et al.*²⁴ for BeSe. The latter calculations largely overestimate the stiffness of the BeSe crystal, probably due to the attribution of the Se3d states to the core. As the treatment of Zn3d (and also preferably Se3d) as valence states is now recognized as essential in pseudopotential calculations for achieving good description of elastic properties of ZnSe, an overall agreement is established between state-of-art LDA calculations. Fig. 1 shows the total energy profiles, as function of uniform lattice scaling (left panels) and in its dependency on the off-center displacement (along any Cartesian direction) of one sublattice (anions or cations) relative to the other, i.e., the zone-center TO mode (right panels). The energy vs. lattice constant curves from all-electron WIEN2k calculations and from SIESTA are almost identical. Small kinks in the SIESTA total energy plot at some values of lattice constant are due to changes of the real-space mesh for spatial integration (as the cell volume varies but the mesh density is maintained about the same). The energy profiles of the anion-cation displacement (TO phonon, see right panels of Fig. 1) shows no substantial anharmonicity (deviations from parabolic behavior) for both ZnSe and BeSe. The phonon frequencies in Table I were calculated from the second-order fit to these data. Phonon frequencies in the following sections result from the diagonalization of dynamical matrices, constructed

from the forces induced on atoms by small Cartesian displacements. For pure constituents they agree very well with the results of the second-order total energy fit. It is noteworthy that a big difference in Γ -TO frequencies of ZnSe and BeSe is only in part due to a large differences in the cation masses. The force constants are larger in BeSe, as is well seen from Fig. 1, indicating higher stiffness of this material, also manifested in its larger bulk modulus.

Some our results listed in Table 1 are slightly refined as compared to those reported earlier in Ref. 4, due to an use of a more recent realization of the all-electron method (WIEN2k instead of WIEN97), and a more extended basis set in SIESTA.

In the discussion of phonon properties below we refer to dispersion curves of ZnSe (obtained from neutron scattering and calculated in the rigid ion model, Ref. 28) and BeSe (calculated using self-consistent pseudopotential method and linear response approach, Ref. 29). A recent calculation³⁰ of phonon dispersion for both systems based on a simple model with central and angular forces yields acceptable results for ZnSe but large difference from *ab initio* phonon dispersion curves for BeSe. This could be a manifestation of more covalent character of bonding in BeSe, as discussed below.

IV. BOND LENGTHS IN MIXED CRYSTALS

In a sequence of supercell calculations which represent mixed Be-Zn compositions, we begin by unconstrained relaxation of lattice vectors and internal coordinates. Probably the simplest model of a mixed system with predominantly either Be or Zn at cation sites is an ordered

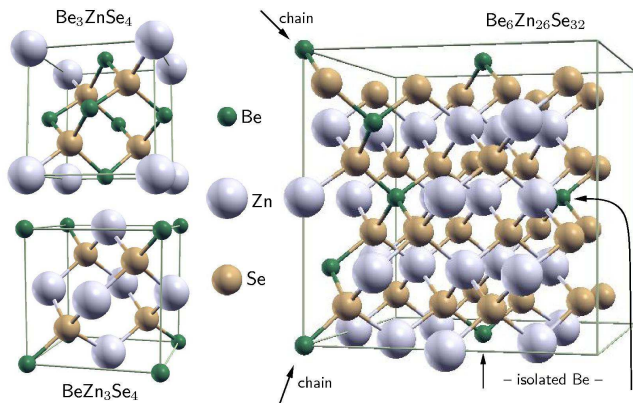


FIG. 2: Cubic supercells used in the calculation. The continuous Be–Se chain and isolated Be atoms are marked in the large supercell. The figure was created with the XCrySDen software³¹.

8-atom superstructure with the cubic primitive cell. Such supercells BeZn_3Se_4 and Be_3ZnSe_4 are shown in the left-hand side of Fig. 2. We emphasize that the BeZn_3Se_4 superstructure contains Be atoms only in configuration which will be further referred to as “isolated” one; i.e., each Se neighbor to a Be atom has only Zn ions to saturate its other bonds. In the Be_3ZnSe_4 superstructure, on the contrary, each Se ion has but a single Zn neighbor, whereas Be–Se bonds form a continuous framework throughout the crystal.

In order to better understand the changes of the phonon spectra in presumed dependency on the percolation setup, we performed the lattice dynamics simulation in a larger $2 \times 2 \times 2$ (64 atoms) supercell. It contained 4 beryllium atoms in a continuous –Be–Se– chain transversing the crystal; moreover, two other Be atoms were situated in “isolated” positions, with only their fifth-nearest neighbors being of the Be type. This supercell is also shown in Fig. 2. When fully relaxed, it maintains a nearly cubic shape, with a tiny z -compression ($c/a=0.998$) due to the anisotropy of chains. The nominal composition of Be is 18.75 at.%, i.e. just below the theoretical percolation threshold (0.198) on the fcc lattice³²; however, our structure includes percolation on the Be sublattice by construction. The advantage of our choice of supercell is that, despite its relatively moderate size, it allows to analyze local properties of areas with percolation (chained Be–Se bonds) or without percolation (isolated Be–Se bonds only) on equal footing. The results for this supercell will constitute the bulk of our discussion on the lattice dynamics.

We note in passing that possible manifestation of percolation effects in mixed semiconductor systems, notably at the above critical concentration and especially in systems with large contrast in stiffness, has been pointed at by Bellaiche *et al.* already some time ago³³.

Finally, four supercells $\text{Be}_n\text{Zn}_{32-n}\text{Se}_{32}$ ($n=1, \dots, 4$) of the same size and cubic shape as the latest one simulate a gradual aggregation of Be ions neighboring *the same*

anion site.

Fig. 3 shows the equilibrium lattice constant (derived from the relaxed supercell volume) and the mean cation–anion bond lengths. The mean lattice parameter exhibits a markedly linear dependence on the concentration. At the same time, the Zn–Se and Be–Se bond lengths tend to remain nearly constant throughout the whole concentration range. A similar conclusion follows from the MD simulations for the (Ga,In)As system by Brancio *et al.*⁵, who also cite EXAFS data, agreeing well with their results, and for the (Be,Zn)Se alloy – by Tsai *et al.*⁶, also based on MD simulations. However, the later publication reports a seemingly too large drop in the Be–Se distance when going from $\text{Zn}_{1/4}\text{Be}_{3/4}\text{Se}$ to pure BeSe. It should be noted that Tsai *et al.* found much smaller difference between the Zn–Se and Be–Se bond lengths than in our case, moreover their lattice parameters for pure constituents considerably deviate from experiment, probably, due to insufficiency of the basis set (and/or pseudopotential) they used.

The diversity of local order in a mixed crystal com-

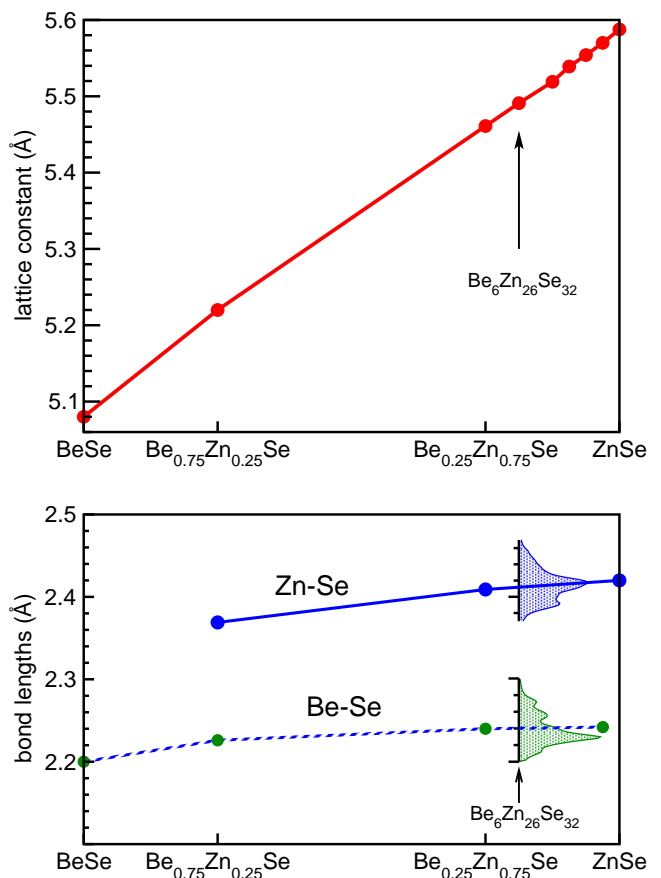


FIG. 3: Top panel: calculated equilibrium lattice constant in $\text{Be}_x\text{Zn}_{1-x}\text{Se}$ crystals of different concentration, represented by supercells (see text for details). Bottom panel: equilibrium Be–Se and Zn–Se bond lengths. For $x=0.19$, the bond length values show a scattering due to the presence of different local environments – see details in the text and in Fig. 4.

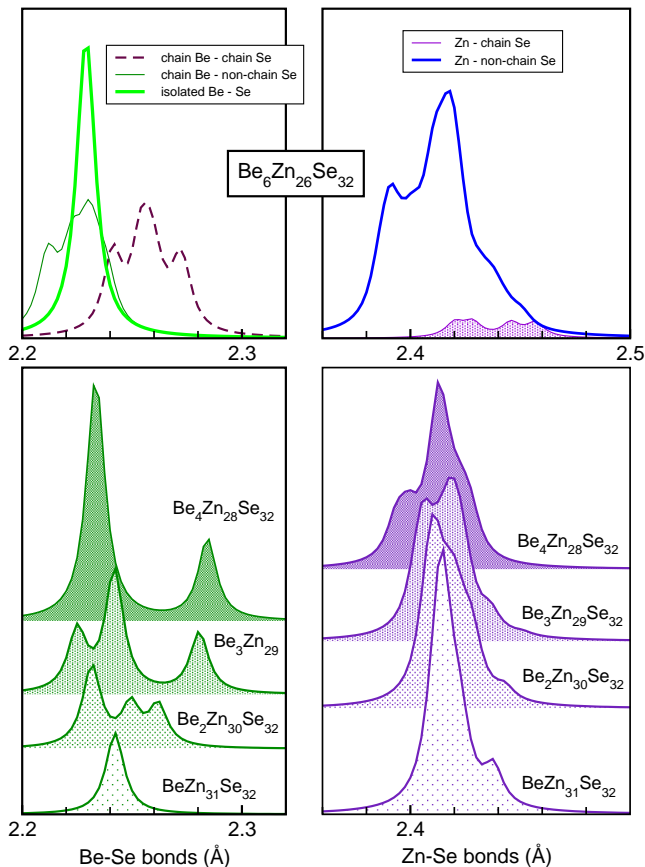


FIG. 4: Bond lengths in relaxed (Be,Zn)Se supercells; A discrete set of 128 nearest-neighbor distances is artificially smeared for better visibility. Top panels: bond lengths in the “model” supercell, with four Be atoms in continuous Be–Se chains, and two isolated Be impurities. Distances between different types of anions and cations are shown separately. Bottom panels: Be–Se and Zn–Se interatomic distances in four supercells, containing one to four Be atoms, neighboring the same Se atom.

petes with the tendency to maintain the bond lengths, with the effect that the latter get a certain scattering around their mean values. This is illustrated in Fig. 3 for the $\text{Be}_6\text{Zn}_{26}\text{Se}_{32}$ supercell, and in more detail for this and other “large” supercells – in Fig. 4. A discrete “spectrum” of, in total, 128 bond lengths in each fully relaxed supercell is artificially broadened there for better visibility. We start our discussion from the $\text{BeZn}_{31}\text{Se}_{32}$ supercell. Four Se neighbors experience an inward relaxation to a single Be impurity, shortening the Be–Se bonds to about 2.24 \AA , i.e., only slightly larger than in pure BeSe. Simultaneously the bonds to their Zn neighbors extend beyond the average interatomic distance ($\sim 2.41 \text{ \AA}$) in the rest of the predominantly-ZnSe supercell. By gradually adding more Be neighbors which share the same Se atom, we end up with a symmetric relaxation pattern in $\text{Be}_4\text{Zn}_{26}\text{Se}_{32}$ with a set of 12 contracted bonds (between Be and their outer Se neighbors) and 4 ex-

tended bonds (from each Be to the central Se). This is clearly seen in Fig. 4. The intermediate cases of 2 and 3 Be atoms in the supercell offer an interpolation between the two discussed cases, introducing a diversity in the Be–Se bond lengths depending on the type of second neighbors. The splitting of the Be–Se bonds into shorter and longer ones, around the mean value of $\sim 2.24 \text{ \AA}$, leads to the diversification of the Zn–Se bonds into, correspondingly, longer and shorter ones, as compared to the dominating bulk-ZnSe central peak at $\sim 2.41 \text{ \AA}$. A more complex distribution of bond lengths comes about in a supercell which contains, along with isolated Be impurities, a continuous –Be–Se– chain (Fig. 4, top panels). A Be atom substituting Zn favors an inward relaxation of neighboring Se. Large enough around a zero-dimensional defect (isolated atom), such inward relaxation is even stronger around a one-dimensional defect, such as an extended –Be–Se– chain. The tendency for shortening the Be–Se bond lengths should obviously exist also along the chain, but the actual contraction is limited by the fact that the chain is quasi-infinite and embedded into the ZnSe lattice, which effectively fixes the chain’s step. However, since the repeated cation-anion sequence in the zincblende structure is folded, the shortening of its links can be achieved by accommodating the interbond angles, at the price of stretching the bonds between the in-chain Se atoms and their Zn neighbors in the crystal (shaded area in the top right panel of Fig. 4). The distribution of bond lengths between Zn cations and the off-chain Se anions resembles roughly that in the chain-free $\text{Be}_4\text{Zn}_{28}\text{Se}_{32}$ supercell.

V. FORCE CONSTANTS

We look now at how the variations in bond lengths map onto changes in the force constants. As already mentioned, the latter become accumulated as we displace the atoms one by one from their equilibrium positions along three Cartesian directions and analyze the forces induced on all atoms of the supercell. Specifically (in the symmetrized form),

$$D_{ij}^{\alpha\beta} = -\frac{1}{2} \left[\frac{F_i^\alpha(\{\mathbf{R}\} + d_j^\beta) - F_i^\alpha(\{\mathbf{R}\} - d_j^\beta)}{2d_j^\beta} + \frac{F_j^\beta(\{\mathbf{R}\} + d_i^\alpha) - F_j^\beta(\{\mathbf{R}\} - d_i^\alpha)}{2d_i^\alpha} \right] \quad (1)$$

where F_i^α is the force on atom α in the direction i , and $\{\mathbf{R}\} + d_j^\beta$ means that of all atoms, only the atom β is displaced along j from its equilibrium position, by (in our case) $d=0.03$ Bohr. With all elements of $D_{ij}^{\alpha\beta}$ recovered, the solution of dynamical equation

$$\sum_{\beta,k} \left[\omega^2 \delta_{\alpha\beta} \delta_{ik} - \frac{D_{ij}^{\alpha\beta}}{\sqrt{M_\alpha M_\beta}} \right] A_k^\beta = 0 \quad (2)$$

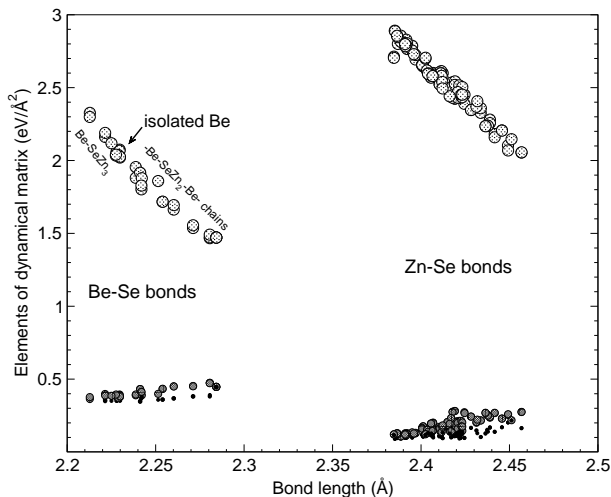


FIG. 5: Diagonal elements of force constant matrix between nearest neighbors. See text for details.

yields zone-center phonon frequencies ω and eigenvectors A_i^α of the supercell. Before turning to the analysis of phonons, we discuss briefly the force constants $D_{ij}^{\alpha\beta}$. For each atomic pair $\{\alpha, \beta\}$, they make a 3×3 matrix which can be diagonalized. The diagonal elements are shown in Fig. 5 in dependency on the corresponding interatomic distance. In accord with previously discussed scattering of the Be–Se and Zn–Se bond lengths, we have now a scattering of force constants. The major elements (of diagonalized 3×3 matrix) show a remarkably pronounced linear variation with the bond length. Two minor elements are much smaller in magnitude and roughly bondlength independent. One can interpret the smallness of minor elements of $D^{\alpha\beta}$ as a measure of the covalency of corresponding bonds. Indeed, in case of a purely ionic bonding only the central motion of atoms would bring about a change in the force; the tangential component makes a non-zero contribution to the force constant only if tangential displacement induces a redistribution of charge density, meaning that the covalency of the bond is not negligible. The contrast between strongly anisotropic and hence essentially ionic force constants for the Zn–Se bonds and much more covalent Be–Se interaction is clearly seen in Fig. 5. It is remarkable that the central Be–Se interaction is, on the average, smaller than the Zn–Se one. Yet, we have seen that the BeSe crystal possesses larger bulk modulus and a higher elasticity parameter in the Γ -TO vibration. This can only be explained by a considerable contribution of non-central forces (minor elements of the force constants) in the shaping of such elastic parameters. In other words, whereas in ZnSe the stretching of Zn–Se bonds plays a dominant role in the elasticity, in BeSe the bending of bond angles is nearly as important.

We find very remarkable a pronounced linear dependence of the force constants on the interatomic distance, in apparent indifference to other aspects of the local or-

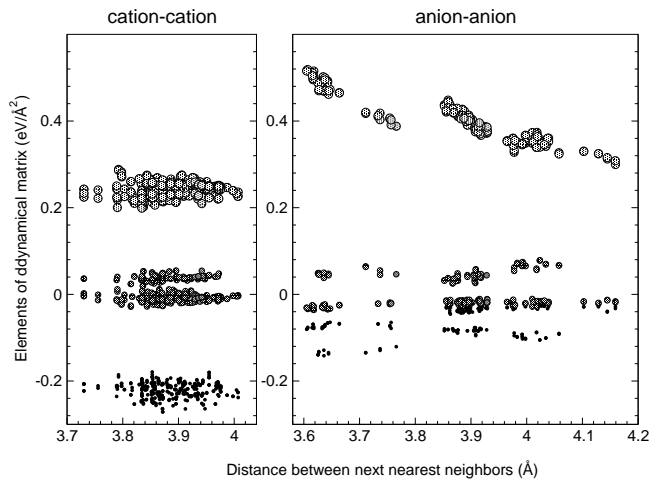


FIG. 6: Diagonal elements of force constant matrix between next nearest neighbors. Left panel: (Be,Zn)–(Be,Zn); right panel: Se–Se.

der. The obtained dependence can be parametrized and used for fast lattice-dynamics simulations in much larger supercells. The results for similarly diagonalized second-nearest neighbors interaction are shown in Fig. 6. The scattering of the Se–Se distances is twice as large as that of cation-cation ones, and shows a clear splitting into two groups, similar to that reported in Ref. 5 for the As–As pair distribution function in (Ga,In)As. This means that Be substitutes Zn almost at their original (non-displaced) positions, i.e., the cation sublattice remains rather rigid, whereas the Se atoms undergo large displacements, depending on their local environment. We see a pronouncedly different behavior of cation-cation and anion-anion force constants: the former have two almost symmetric (positive/negative) diagonal elements, with the third being nearly zero, independently on both type of pair (Be–Be, Be–Zn or Zn–Zn) and on the distance. The anion-anion coupling has an appreciable central-force element, decreasing with the distance, and two much smaller tangential elements. The variation of the major element with distance is (at least in part) related to the fact that on the left hand side of the plot we deal mostly with Se–Be–Se connections, in which the central Se–Se interaction reflects the effect of bending the strongly covalent Be–Se bonds; on the right hand site, the Se–Zn–Se connections offer a much weaker resistance to such bending, due to a higher bond ionicity.

VI. PHONONS

Since we deal with relatively large “disordered” supercells with no internal (short-scale) periodicity, and no clear-cut phonon dispersion exists in such systems, it does not make sense to Fourier-transform the force constants (1) prior to solving the dynamical equation (2). However, we explain below how to extract some

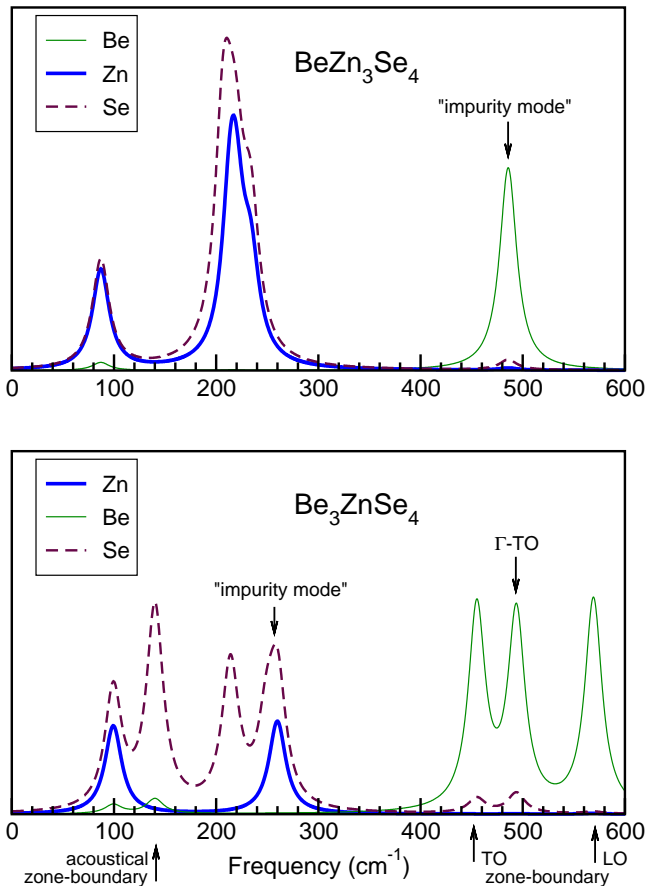


FIG. 7: Phonon density of states for the BeZn_3Se_4 and Be_3ZnSe_4 supercells, calculated for $q=0$ of the supercell and broadened by 10 cm^{-1} .

q -resolved information about lattice vibrations. The primary characteristic for our discussion will be the phonon density of states (PhDOS), resolved when necessary over freely chosen groups \aleph of atoms α :

$$I_{\aleph}(\omega) = \sum_{\alpha \in \aleph} \sum_i |A_i^\alpha(\omega)|^2. \quad (3)$$

This is a discrete spectrum of $(3N - 3)$ lines (for N atoms in the supercell, with acoustic modes removed) of different intensity, which is in the following figures broadened with the halfwidth parameter of 10 cm^{-1} , for better visibility. The vibration modes obtained from the solution of Eq. (2) correspond to the zone-center of the supercell in question, but they reflect different vibration patterns, also those of non-zone-center character, with respect to the underlying zincblende lattice. Let us discuss this for 8-atom supercells, whose calculated PhDOS is shown in Fig. 7.

The $q=0$ vibration modes in a supercell include the “true” zone-center phonon (relative to the basic zincblende cell), as well as zone-boundary phonons backfolded to a smaller BZ of the superstructure. It is relatively easy to distinguish them by their eigenvectors;

certain modes are labeled in Fig. 7. Most obviously, the acoustical branch hits the BZ boundary at 87 cm^{-1} (Zn-rich system) or 140 cm^{-1} (Be-rich system). As ranges of frequencies of Be-related and Zn-related optical modes are well separated, due to a large difference in masses, it is straightforward to recognize the BeSe-type Γ -TO mode at 494 cm^{-1} (lower panel of Fig. 7), the backfold of the optical branch at the zone boundary at 450 cm^{-1} , and the backfold of the zone-boundary longitudinal phonon at 560 cm^{-1} – all in good agreement with the linear-response phonon dispersions calculated for BeSe by Tuntuncu *et al.*²⁹ The zone-center LO mode is not present, because we do not include macroscopic electric field in crystal in our calculation. In the Zn-rich crystal, the Be-related TO mode (at 487 cm^{-1}) behaves like an impurity mode and exhibits no dispersion. Whereas the Zn-related mode is similarly dispersionless (at 260 cm^{-1}) in the Be-rich system, in BeZn_3Se_4 the ZnSe-related TO branch shows dispersion, manifested by backfolding of zone-boundary phonon and hence additional structure at $200\text{--}240 \text{ cm}^{-1}$, in agreement with experiments and calculations of Refs. 28,30.

Even as these 8-atom supercells may be too simplistic to imitate short-range order effects in real quasibinary alloy, they exhibit important features which also persist in more sophisticated representative structures: a difference between dispersionless modes due to “isolated” impurities and dispersing modes due to continuous connected chains; a more pronounced dispersion in BeSe-related modes than in much softer ZnSe-related ones.

We turn next to the discussion of phonons in a larger $\text{Be}_6\text{Zn}_{26}\text{Se}_{32}$ supercell. There are now more lines in the spectrum, and, as the Brillouin zone (BZ) becomes smaller, the Γ modes of the supercell offer a sampling over more non-zone-center modes in a zincblende lattice. This leads in more features and more “filled” form of the PhDOS (Fig. 8).

The vibration spectra of both pure systems ZnSe and BeSe are shaped by broad acoustical branches and more narrow optical ones. In ZnSe they nearly overlap, resulting in a characteristic two-peaked structure of the PhDOS – see, e.g., Hennion *et al.*²⁸. Our low-frequency (ZnSe-related, up to 300 cm^{-1}) part of the supercell PhDOS provides a fair agreement with this known result for pure ZnSe. The spectrum of BeSe has a large separation between its acoustical and optical parts. The former covers the whole region of the phonon spectrum of ZnSe. Therefore, in a mixed crystal, the partial PhDOS of Se atoms which have four Zn neighbors essentially repeats the shape of the Zn PhDOS, whereas those Se atoms with one or two Be neighbors participate in vibrations at $100\text{--}200 \text{ cm}^{-1}$, i.e., in the “pseudogap” region of ZnSe. These modes have mostly acoustical character.

We consider now more attentively the high-frequency optical modes with high participation of Be vibrations. The corresponding PhDOS (Fig. 8, top panel) is separated into contributions from (two) “isolated Be” atoms and those (four) in the infinite chain. The “isolated Be”

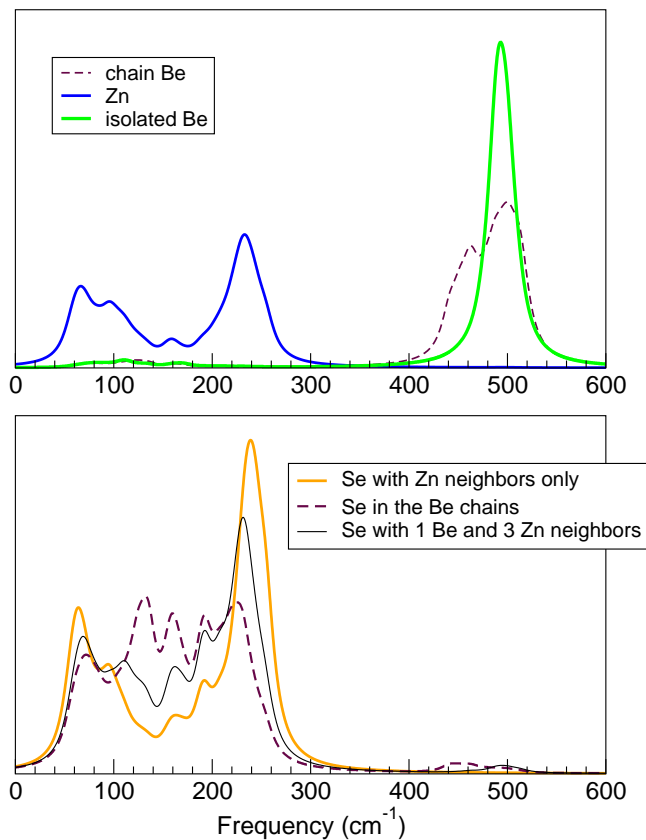


FIG. 8: Phonon density of states for the $\text{Be}_6\text{Zn}_{26}\text{Se}_{32}$ supercell, resolved over different groups of atoms, calculated for $q=0$ of the supercell and broadened by 10 cm^{-1} . The vertical scaling for different groups is arbitrary.

contribution is, expectedly, a single narrow line, coming about from several nearly degenerate vibration frequencies. The vibrations of Be in the chains are more diversified: the characteristic frequencies can be found below, within and above the “isolated Be” peak. The most remarkable is a clear split off at a soft side, which makes a distinguished peak in the vibration spectrum, similar to that experimentally observed in samples with a presumed percolation on the Be sublattice^{2,19}. The previous discussion on the distribution of bondlengths, and the force constants’ dependence on the latter, helps us to understand this behavior. The bonds between the chain Be atoms and *out-of-chain* Se are shorter than those involving isolated Be, and corresponding force constants are larger. On the contrary, the Be–Se bonds *along the chain* are less contracted; the longer bond length implies smaller force constant hence lower vibration frequency. Our explanation of the experimentally observed anomalous (split-off) Be mode is, therefore, the following. As the concentration of Be in ZnSe reaches the percolation limit and infinite chains are built, the Be–Se bonds in these chains are forced to become longer than around isolated Be impurities, or in short chain fragments. This immediately softens the vibration modes which involve

such extended bonds.

In order to extend this interpretation over experimentally measured Raman lines, which are known to scan primarily the zone-center phonons, one needs yet to extract a wavevector-resolved information about calculated vibrations. As the supercell size increased, the effective sampling over the Brillouin zone (BZ) of the basic zincblende lattice became more fine. In particular, one has not only X , K and L zone-boundary phonons sampled, as was the case for the 8-atom cells, but also q points halfway to them from the zone center. We mentioned already that the lack of translation symmetry in the mixed BeSe–ZnSe supercell does not allow to Fourier transform the dynamical matrix and arrive at neat phonon dispersion curves. However, one can project the dispersion patterns, corresponding to different modes of vibration, onto the plane wave with different q values and in such way define q -resolved contributions to the phonon DOS:

$$I_{\mathbb{N}}(\omega, \mathbf{q}) = \sum_{\alpha \in \mathbb{N}} \sum_i |A_i^\alpha(\omega) \exp(i\mathbf{q}\mathbf{R}_\alpha)|^2. \quad (4)$$

Since eigenvectors correspond to $q=0$ of the supercell and hence are real, the phase of the plane wave has no importance. One can view $I_{\mathbb{N}}(\omega, \mathbf{q})$ as spectral function, which in principle would show how the phonon dispersion bands of pure constituents get overlapped, distorted and smeared in a mixed crystal. Unfortunately, the results obtained for our – yet relatively small – 64-atom supercell do not allow to see anything resembling a continuous displacement of intensity maxima with q ³⁴. Nonetheless, we present in Fig. 9 the projected PhDOS for three q values along the (001) direction. The ZnSe-type vibrations make clearly visible the displacement of two acoustical bands, known, e.g., from the measured phonon dispersion curves²⁸, as the projection wavevector changes from the zone-center via midpoint to the zone boundary.

For the Be-related modes, because of small amount of Be atoms in the supercell, the dispersion is generally less pronounced, yet noticeable in the (001) direction, which is the general direction of the chains. Being almost non-interacting linear defects, the chains do not give rise to noticeable dispersion in perpendicular directions. The three acoustical modes, removed in the previous PhDOS figures, are retained in Fig. 9, in order to show how the spectral weight of the $\omega=0$ modes disappears for q values away from zero. A notable difference is the PhDOS of isolated Be, which is nearly identical for $q=0$ and $q=(001)$. This is because the supercell contains two isolated Be atoms. They interact only weakly but create a superstructure that effectively halves the BZ in the z direction.

The q -resolving of the PhDOS singles out the modes which are likely to dominate the Raman spectra. The separation into $q=0$ and non- $q=0$ modes is however not very clear-cut – in part due to physical reasons (mixed crystal, loss of periodicity) and in part due to technical limitations (small size of supercell and hence non-vanishing $q=0$ projection of many modes due to numerical noise). One can expect better contrast in selecting

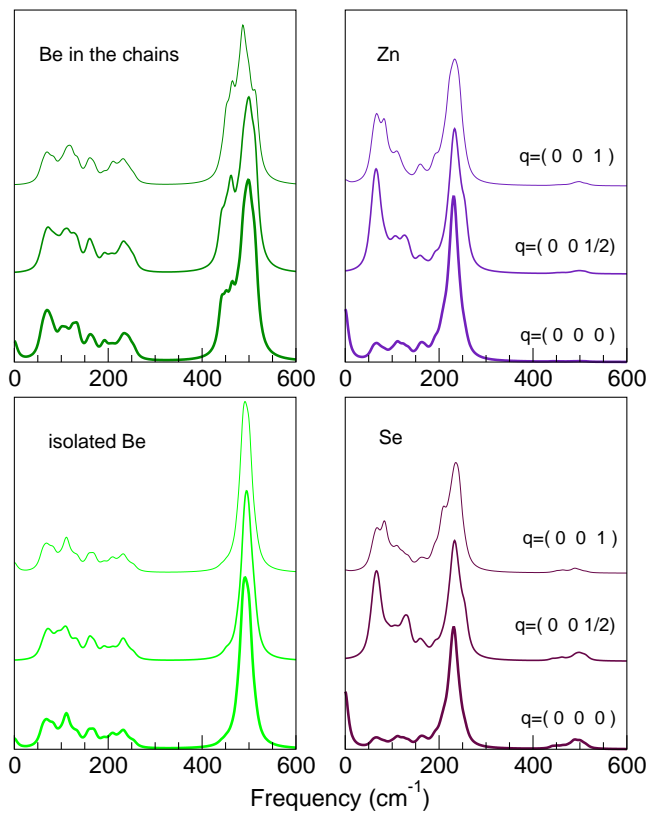


FIG. 9: Phonon spectral function in the $\text{Be}_6\text{Zn}_{26}\text{Se}_{32}$ supercell, corresponding to three values of q of the basic zincblende lattice, broadened by 10 cm^{-1} .

$q=0$ modes in a larger supercell, due to better sampling. Nevertheless, it is clear that the separation into “isolated Be” and “Be in the chains” modes occurs not only on the average over the BZ, but is actually even more pronounced in the zone-center modes. Therefore, our explanation of anomalous Raman lines will hold.

Most of the modes are of very mixed character, and involve stretching and bending of bonds in a complicated manner. However, we selected several ones, involving the $-\text{Be}-\text{Se}-$ chains, whose vibration pattern can be described with relative simplicity. Two of these modes (441 and 452 cm^{-1}) lie in the “anomalous” Raman line, where the vibrations of isolated Be atoms are negligible. Three other selected modes, at 485 , 495 and 502 cm^{-1} , involve simultaneous vibration of all Be atoms, in the chains as well as isolated ones. Fig. 10 gives a snapshot of these five modes. Displacement patterns in some other modes are shown in Fig. 5 of Ref. 4. The vibrations of predominantly “impurity Be” character, leaving the chain Be atoms silent, occur at nearly 490 cm^{-1} , in between the third and the fourth of depicted modes.

The most general observation is that the “anomalous” modes with reduced frequencies involve nearly in-plane displacement of Be with its own equilibrium position and its two Se neighbors. Such motion stretches or shortens the Be–Se bonds but roughly preserves the Be–Se–Be an-

gles. The 441 cm^{-1} mode is a wave of correlated Be displacement along the chain, periodic with the chain step. This is a predominantly Γ mode. The 452 cm^{-1} mode has similarly “longitudinal” character but the doubled translation length: two Be atoms approach, or depart from, their common Se neighbor symmetrically. Consequently this is not a clear zone-center vibration, however due to the curvature of the chain and a complexity of detailed displacement pattern it provides a $\mathbf{q}=0$ contribution in the analysis according to Eq. (4).

The harder modes are related to out-of-plane Be vibrations and hence bending of covalent Be–Se bonds. Somehow simplifying, in the “anomalous modes” there are primarily central Be–Se forces at work, so the frequency is lower than that involving an isolated Be impurity – in accord with longer anion-cation distance along the chain, as illustrated by Fig. 5. In the latter case, even as interatomic distances remain the same, the off-center contributions due to the bond bending effectively increase the force constants and harden the resulting frequency beyond those for an isolated Be.

VII. CONCLUSIONS

We simulated the equilibrium structure and lattice dynamics from first principles in a series of supercells simulating mixed (Be,Zn)Se crystals. We found a nearly linear dependence of equilibrium lattice constant with composition, but a relative independence of (average) Be–Se and Zn–Se distances on concentration. When incorporated in a mixed crystal, the individual interatomic distances develop a certain scattering around their mean values, maintaining however a clear separation between the Be–Se and Zn–Se bond lengths. Specifically, an isolated Be atom may much more efficiently shorten the bonds to an Se neighbor whose other three bonds are Zn-terminated, than to an Se atom shared by other Be neighbors. In particular, a continuous $-\text{Be}-\text{Se}-$ chain is characterized by longer link lengths than the average Be–Se distance, for a given concentration. We demonstrated further that this has effect on force constants and vibration frequencies. As follows from our direct calculation of interatomic force constants, the principal values of the latter, taken as diagonal elements of a 3×3 matrix relating two selected atoms, show a linear decrease as a function of cation-anion distance between nearest neighbors. The calculations manifest a primarily ionic character of the Zn–Se interaction and a remarkable level of covalency in the Be–Se bonds. A decrease of force constants with larger bond distance is the microscopic origin of the formation of a softened “anomalous” mode, which appears on the low-frequency side of BeSe-related TO mode. Our wavevector analysis of vibration patterns in the supercell indicates that the “anomalous” mode has a strong zone-center contribution, that is consistent with its clear experimental observation in the Raman spectra. We confirmed therefore on the microscopic level the early

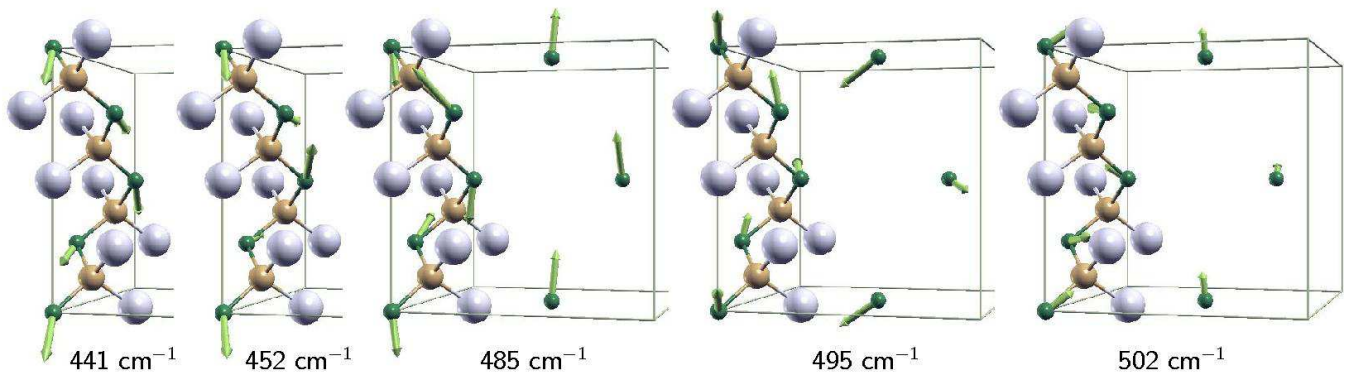


FIG. 10: Vibration patterns of five selected modes with substantial contribution of Be atoms; the relative displacements of the latter are shown by arrows. Only some atoms of the $\text{Be}_6\text{Zn}_{26}\text{Se}_{32}$ supercell (Fig. 2, right panel) are shown. The figure was created with the XCRYSDEN software³¹. The first two modes affect exclusively the continuous $-\text{Be}-\text{Se}-$ chains; the last three contain also comparable contribution of impurity Be atoms. See text for details.

presumed relation between the onset of Be percolation threshold on the cation sublattice and the appearance of “anomalous” mode, including specific vibrations of continuous $-\text{Be}-\text{Se}-$ chains transversing the crystal.

Acknowledgments

A.V.P. thanks the Université Metz for invitation for a research stay there and the hospitality of the Institut

de Physique. Useful comments by N. E. Christensen, discussions with V. Vikhnin and travel support from the NATO project CLG 980378 are greatly appreciated.

-
- * Electronic address: apostnik@uos.de
- ¹ C. Chauvet, E. Tournié, and J.-P. Faurie, *Phys. Rev. B* **61**, 5332 (2000).
 - ² O. Pagès, M. Ajjoun, D. Bormann, C. Chauvet, E. Tournié, and J. P. Faurie, *Phys. Rev. B* **65**, 035213 (2002).
 - ³ O. Pagès, M. Ajjoun, T. Tite, D. Bormann, E. Tournié, and K. C. Rustagi, *Phys. Rev. B* **70**, 155319 (2004).
 - ⁴ A. V. Postnikov, O. Pagès, T. Tite, M. Ajjoun, and J. Hugel, to be published in *Phase Transitions* (2005), <http://xxx.lanl.gov/abs/cond-mat/0404359>.
 - ⁵ P. S. Branicio, R. K. Kalia, A. Nakano, J. P. Rino, F. Shimajo, and P. Vashishta, *Appl. Phys. Lett.* **82**, 1057 (2003).
 - ⁶ M.-H. Tsai, F. C. Peiris, S. Lee, and J. K. Furdyna, *Phys. Rev. B* **65**, 235202 (2002).
 - ⁷ J. M. Soler, E. Artacho, J. D. Gale, A. García, J. Junquera, P. Ordejón, and D. Sánchez-Portal, *J. Phys.: Condens. Matter* **14**, 2745 (2002).
 - ⁸ D. Sánchez-Portal, E. Artacho, and J. M. Soler, *J. Phys.: Condens. Matter* **8**, 3859 (1996).
 - ⁹ J. Junquera, Ó. Paz, D. Sánchez-Portal, and E. Artacho, *Phys. Rev. B* **64**, 235111 (2001).
 - ¹⁰ N. Troullier and J. L. Martins, *Phys. Rev. B* **43**, 1993 (1991).
 - ¹¹ D. J. Singh, *Planewaves, pseudopotentials and the LAPW method* (Kluwer Academic Publishers, Boston, 1994).
 - ¹² P. Blaha, K. Schwarz, G. K. H. Madsen, D. Kvasnicka, and J. Luitz, *WIEN2k, Vienna University of Technology* (2001), improved and updated Unix version of the original copyrighted WIEN-code, which was published by P. Blaha, K. Schwarz, P. Sorantin, and S. B. Trickey, in *Comput. Phys. Commun.* **59**, 339 (1990), URL <http://www.wien2k.at>.
 - ¹³ J. P. Perdew, K. Burke, and M. Ernzerhof, *Phys. Rev. Lett.* **77**, 3865 (1996).
 - ¹⁴ G.-D. Lee, M. H. Lee, and J. Ihm, *Phys. Rev. B* **52**, 1459 (1995).
 - ¹⁵ B. K. Agrawal, P. S. Yadav, and S. Agrawal, *Phys. Rev. B* **50**, 14881 (1994).
 - ¹⁶ A. Fleszar and W. Hanke, *Phys. Rev. B* **62**, 2466 (2000).
 - ¹⁷ K.-H. Hellwege and O. Madelung, eds., *Semiconductors. Physics of II-VI and I-VII Compounds*, vol. 17, Part b of *Landolt-Börnstein, New Series, Group III* (Springer, Berlin, 1972).
 - ¹⁸ B. H. Lee, *J. Appl. Phys.* **41**, 2988 (1970).
 - ¹⁹ O. Pagès, M. Ajjoun, J. P. Laurenti, D. Bormann, C. Chauvet, E. Tournié, and J. P. Faurie, *Applied Physics Letters* **77**, 519 (2000).
 - ²⁰ M. Szybowicz, M. Kozielski, F. Firszt, S. Łęgowski, and H. Męczyńska, *Crystal Research and Technology* **38**, 359 (2003).
 - ²¹ H. Luo, K. Ghandehari, R. G. Greene, A. L. Ruoff, S. S. Trail, and F. J. DiSalvo, *Phys. Rev. B* **52**, 7058 (1995).
 - ²² B.-H. Cheong, C. H. Park, and K. J. Chang, *Phys. Rev. B* **51**, 10610 (1995).
 - ²³ A. Muñoz, P. Rodríguez-Hernández, and A. Mujica, *Phys. Rev. B* **54**, 11861 (1996).

- ²⁴ M. González-Díaz, P. Rodríguez-Hernández, and A. Muñoz, Phys. Rev. B **55**, 14043 (1997).
- ²⁵ L. Muratov, S. Little, Y. Yang, B. R. Cooper, T. H. Myers, and J. M. Wills, Phys. Rev. B **64**, 035206 (2001).
- ²⁶ A. Fleszar, Phys. Rev. B **64**, 245204 (2001).
- ²⁷ W. Luo, S. Ismail-Beigi, M. L. Cohen, and S. G. Louie, Phys. Rev. B **66**, 195215 (2002).
- ²⁸ B. Hennion, F. Moussa, G. Pepy, and K. Kunc, Physics Letters **36A**, 376 (1971).
- ²⁹ H. M. Tutuncu, J. S. Tse, and G. P. Srivastava, in *Phonons in Condensed Materials*, edited by S. P. Sanyal and R. K. Singh (Allied Publishers Pvt. Limited, New Delhi, Mumbai, Kolkata, Lucknow, Chennai, Nagpur, Bangalore, Hyderabad, Ahmedabad, 2004), pp. 38–42.
- ³⁰ S. Doyen-Lang, O. Pages, L. Lang, and J. Hugel, Physica Status Solidi (b) **229**, 563 (2002).
- ³¹ A. Kokalj, Journal of Molecular Graphics and Modelling **17**, 176 (1999), code available from <http://www.xcrysden.org>.
- ³² D. Stauffer and A. Aharony, *Introduction to Percolation Theory* (Taylor & Francis Ltd., London, Philadelphia, 1998, 2001).
- ³³ L. Bellaiche, S.-H. Wei, and A. Zunger, Phys. Rev. B **54**, 17568 (1996).
- ³⁴ The reason is that only limited number of vibration frequencies is represented in the supercell, and only the weight of different modes but not their frequencies may change in the projection on different q . For instance, there are not enough modes corresponding to the gradual rise of acoustical branches towards the zone boundary. As a consequence, the phonon DOS plotted in the (q, ω) -domain shows a step-like rather than smooth change.